Physics and Imaging in Radiation Oncology 24 (2022) 111–117

Contents lists available at ScienceDirect

Physics and Imaging in Radiation Oncology

journal homepage: www.sciencedirect.com/journal/physics-and-imaging-in-radiation-oncology

Original Research Article

Feasibility of artificial-intelligence-based synthetic computed tomography in a magnetic resonance-only radiotherapy workflow for brain radiotherapy: Two-way dose validation and 2D/2D kV-image-based positioning

Siti Masitho *, Juliane Szkitsak, Johanna Grigo, Rainer Fietkau, Florian Putz, Christoph Bert

Department of Radiation Oncology, Universitätsklinikum Erlangen, Friedrich-Alexander-Universität Erlangen-Nürnberg (FAU), Erlangen, Germany
Comprehensive Cancer Center Erlangen-EMN (CCC ER-EMN), Erlangen, Germany

ARTICLE INFO

Keywords:
Brain radiotherapy
Synthetic CT
MRI-only workflow
Artificial intelligence
kV-image-based positioning

ABSTRACT

Background and purpose: Magnetic Resonance Imaging (MRI)-only workflow eliminates the MRI-computed tomography (CT) registration inaccuracy, which degrades radiotherapy (RT) treatment accuracy. For an MRI-only workflow MRI sequences need to be converted to synthetic-CT (sCT). The purpose of this study was to evaluate a commercially available artificial intelligence (AI)-based sCT generation for dose calculation and 2D/2D kV-image daily positioning for brain RT workflow.

Materials and methods: T1-VIBE DIXON was acquired at the 1.5 T MRI for 26 patients in RT setup for sCTs generation. For each patient, a volumetric modulated arc therapy (VMAT) plan was optimized on the CT, then recalculated on the sCT; and vice versa. sCT-based digitally reconstructed radiographs (DRRs) were fused with stereoscopic X-ray images recorded as image guidance for clinical treatments. Dosimetric differences between planned/recalculated doses and the differences between the calculated and recorded clinical couch shift/rotation were evaluated.

Results: Mean ΔD_{50} between planned/recalculated doses for target volumes ranged between −0.2 % and 0.2 %; mean ΔD_{50} and $\Delta D_{0.01ccm}$ were −0.6 % and 1.6 % and −1.4 % and 1.0 % for organ-at-risks, respectively. Differences were tested for clinical equivalence using intervals ±2 % (dose), ±1mm (translation), and ±1° (rotation). Dose equivalence was found using ±2 % interval ($p < 0.001$). The median differences between lat./long./vert. couch shift between CT-based/sCT-based DRRs were 0.3 mm/0.2 mm/0.3 mm ($p < 0.05$); median differences between lat./long./vert. couch rotation were −1.5°/0.1°/0.1° (after improvement of RT setup: −0.4°/−0.1°/−0.4°, $p < 0.05$).

Conclusions: This in-silico study showed that the AI-based sCT provided equivalent results to the CT for dose calculation and daily stereoscopic X-ray positioning when using an optimal RT setup during MRI acquisition.

1. Introduction

In radiation oncology, magnetic resonance imaging (MRI) is mainly used to obtain a more accurate delineation of tumor volumes and organs at risk (OARs) due to its superior soft-tissue contrast [1]. The co-registration of MRI and planning computed tomography (CT) is a standard practice in MRI-based radiotherapy (RT) planning. However, differences in positioning in MRI compared to the planning CT arising because of different imaging setup and immobilization equipment between both imaging modalities as well as daily variations may degrade the MRI-CT registration accuracy, which can be up to 2 mm for brain patient [2], although the use of an optimal registration method and patient setup can improve the registration accuracy [3]. Site-specific MRI-CT registration inaccuracies due to patient positioning have been investigated for various sites [2–5]. The consensus article by Paulson et al. [6] on MRI simulation on RT treatment planning recommended an MRI acquisition in the RT position for most regions, such as pelvis and head and neck. Furthermore, it has also been reported that acquiring brain patients in RT position improved the registration accuracy [3]. Different patient positioning for MRI may lead to different extension

* Corresponding author at: Strahlenklinik, Universitätsklinikum Erlangen, Universitätsstraße 27, 91054 Erlangen, Germany.
E-mail address: siti.masitho@uk-erlangen.com (S. Masitho).

https://doi.org/10.1016/j.phro.2022.10.002
Received 15 June 2022; Received in revised form 12 October 2022; Accepted 17 October 2022
Available online 22 October 2022

angle at the occipito-atlanto-axial joint complex, which may affect the registration accuracy due to rotational errors or non-rigid deformation of infratentorial tissues [1,7]. The registration accuracy is critical, especially for sites with frequently small treatment volumes and tiny margin for uncertainties, such as in the case of intracranial stereotactic radiotherapy, where the clinical target volume (CTV)-planning target volume (PTV) margin can be < 1 mm [8,9]. MRI-only RT eliminates the MRI-CT registration step and minimizes the additional dose exposure from the CT acquisition. In addition, the number of scans can be reduced, and thus patient's convenience is improved [10].

Recent advances in MRI techniques have opened up the possibility of replacing CT with MRI for dose calculation and patient setup verification. However, unlike CT, MRI does not directly provide an electron density map, which is the basis for physical RT treatment planning. Different techniques for generating electron density maps out of MR images, so-called pseudo-CT or synthetic-CT (sCT) have been developed and studied, such as the bulk density-based [11–13], atlas-based, voxel intensity-based [14–17], and lately many deep-learning-based generation techniques [18–22].

The full implementation of sCTs in the clinical workflow requires the sCT to provide Houndsfield-Unit (HU) values for dose calculation. The older sCTs generation techniques have had some drawbacks, e.g. the high number of required MRI sequences prolonging the scan time in the case of voxel-intensity-based techniques, or the inadequacy in reconstructing atypical anatomy for atlas-based algorithms [23]. Deep-learning-based sCT generation techniques may allow the generation of more accurate sCTs based on a low number of MRI sequences, though its feasibility for atypical patient anatomy is yet to be investigated. The sCTs must also be able to generate valid reference data for patient positioning at the linear accelerator. In most studies, the sCTs were matched to Cone-Beam-CTs (CBCT) [24,25], but the use of digitally reconstructed radiographs (DRR) generated from sCTs in combination with planar kV/MV X-ray imaging has also been studied [26]. Yang et al. used ultrashort echo time (UTE)-MRI-based DRRs but their approach did not include the possibility of sCT-based dose calculation [27]. Non-coplanar X-ray has also been used for patient setup verification system. However, to the best of our knowledge, to this date no study regarding the performance of DRRs generated from AI-based sCT on a 2D/2D non-coplanar kV X-ray-based patient setup verification system has been conducted.

The purpose of this study was thus to evaluate a commercial deep-learning-based sCT algorithm based on a single T1-weighted DIXON image [28] for dose calculation in brain radiotherapy. Further, the second aim of this study was to investigate the feasibility of the AI-sCT-based DRRs generation for 2D/2D non-coplanar kV X-ray-based patient setup verification.

2. Material and methods

2.1. Clinical workflow

2.1.1. Study population and study design

Inclusion criteria for the present study were patients with gliomas or brain metastases who received RT treatment at the University Hospital Erlangen in the period between 04/2021 and 03/2022 and were treated at Novalis TX (Brainlab, Munich, Germany). Data of 26 patients were retrospectively evaluated. Treated volumes ranged from small planning target volume (PTV) (0.46 ccm) to whole-brain radiotherapy (WBRT) (see Table 1). Nine out of 26 patients had undergone a preceding brain surgery, which caused alteration to the bone structures.

2.1.2. Imaging acquisition

As part of the treatment protocol, patients were scanned at the MRI and CT before receiving external beam radiotherapy. MRIs were acquired at the MAGNETOM Sola (1.5 T, Siemens Healthineers, Erlangen, Germany) using a dedicated RT setup. The RT setup included the use of a flat RT table-top, an immobilization RT mask system, and a dedicated coil setup of two 18 channels Ultraflex coils (further details see [29]). After 20 patients, refinements were made to the RT mask holder for MRI acquisition to increase rotational accuracy compared to treatment position.

Table 1
Summary of patient characteristics.

Parameter	Specification	Value
Number of patients	Total	26
	Undergone prior surgery	9
Gender	Female	12
	Male	14
Age	Median	65 (range 40–88)
Clinical treatment option	Stereotactic radiosurgery (SRS) (1 Fx)	4
	Fractionated stereotactic radiosurgery (FSRT) (≤12 Fx)	11
	Conventional RT (>12 Fx)	11
PTV volume	Mean	315.32 cc (range 0.46–2082.9 cc)

A single pre-contrast T1-DIXON (1.5 mm × 1.5 mm × 1.5 mm, bandwidth = 510 Hz/px) was acquired as part of the clinical MRI protocol at University Hospital Erlangen. Patient-specific active shimming was activated for all the sequences. Planning CTs (1 mm × 1 mm × 1 mm) were acquired at the Somatom go.openPro (Siemens Healthineers, Erlangen, Germany) within 5 days of the MRI.

2.1.3. Radiation treatment planning

Clinical structures were delineated on the MRI images and transferred to CT after rigid registration of MRI and CT. The clinical treatment planning system (TPS, Raystation v10, Raysearch, Stockholm, Sweden) was used for dose calculation. At the treatment machine, a non-coplanar kV X-ray imaging system was used for patient alignment (ExacTrac v6.0.6, Brainlab, Munich, Germany). The ExacTrac system offers translational and rotational parameters for 6DoF patient positioning [30].

2.2. Generation of sCT based treatment plans

The sCTs were retrospectively reconstructed using syngo.via VB60 RT pro edition (Siemens Healthineers, Erlangen, Germany) with the T1-Dixon in-phase and opp-phase contrast images as input (Fig. 1) with an in-plane resolution of 1 mm × 1 mm. According to [28], the deep learning-based algorithm used a combination of multilayer neural networks to learn sCT reconstruction and was trained on 6486 CT and MRI image pairs and 533 validation sets. The first network segments the MRI in three classes (background, bone, soft tissue), while the second network uses Generative Adversarial Network to generate sCT with continuous HU and discriminates it from a real CT image. In the TPS, the HU look-up table as recommended by the vendor [29] was used. Each sCT was first rigidly registered to the corresponding CT, followed by copying the identical clinical structures from the CT onto the sCT. Auxiliary contours such as RT mask, mask holder, infrared (IR) markers, and couch were omitted since the current analysis considered only the patient. Since these structures were not visible in neither the MRI nor the sCT image, considering these in the analysis would also lead to errors in the analysis. For treatment planning, the same constraints and setups as used for clinical plans were taken. Guidelines for dose constraints were majorly adopted from ref. [31]. Volumetric modulated arc therapy (VMAT) plans were optimized script-based on both CT and sCT to maintain clinical plan quality (target coverage, OAR sparing) and plan complexity.

All procedures performed were in accordance with the ethical standards of the institutional research committee and with the 1964 Helsinki declaration and its later amendments. Patient consent was not required for this retrospective study per institutional policy and in accordance with local legislation (BayKrG Art. 27 (4)).

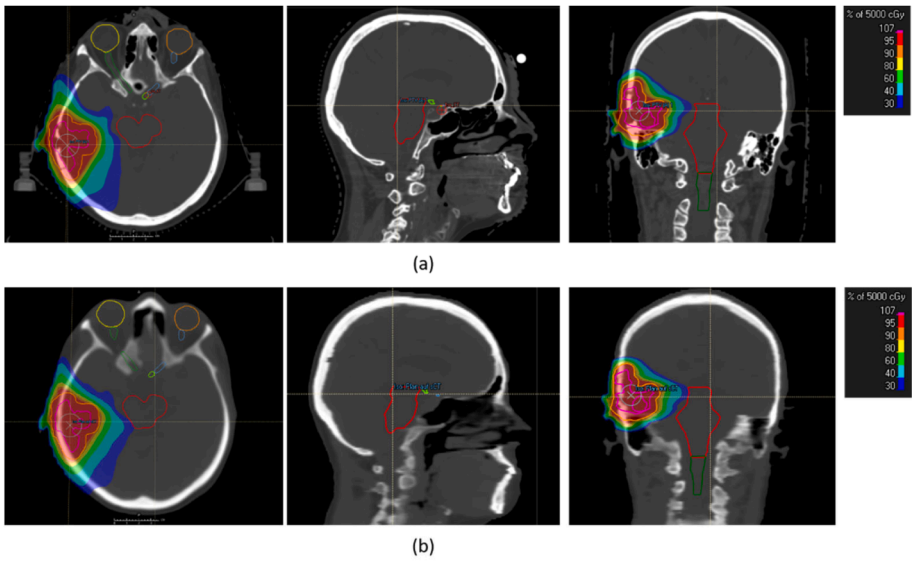

Fig. 1. The colorwash of the planned dose distribution on image datasets. (a) Planned dose distribution on the planning CT and (b) on the reconstructed AI-based synthetic CT of the brain (bone windowing, W = 1600, L = 450).

2.3. Data analysis

HU comparison between CT and sCT was performed. First, the registered sCT was resampled onto the CT using Plastimatch (www.plastimatch.org). Then, the skin contour was defined on the CT and used as a mask for the evaluation, thus excluding voxels outside the region of interest. Mean absolute error (*MAE*) was calculated for all patients.

Dosimetric analysis was performed using a two-way validation: the CT-based VMAT plan was recalculated on the sCT (referred to as $TP_{CT \rightarrow sCT}$); and second, the sCT-based VMAT plan was recalculated on the CT (referred to as $TP_{sCT \rightarrow CT}$). In total, four dose distributions and corresponding Dose-Volume-Histograms (DVH) were obtained (two from the original plans and additional two from recalculation on the other image). The institutional clinical guideline for plan quality judgment was mostly based on the D_{50}, $D_{0.01ccm}$, and PTV coverage (defined as Conformity Index (CI), which is the ratio between the volume covered by the 95 % isodose and the PTV). For the evaluation, the mean percentage deviation of D_{50} (ΔD_{50}[%]) and of $D_{0.01ccm}$ ($\Delta D_{0.01ccm}$[%]), CI, and mean difference (ΔD_{50} and $\Delta D_{0.01ccm}$ in cGy) for PTV, gross tumor volume (GTV), and OARs between original VMAT plan and the recalculated plan were determined. Statistical analysis was performed using a paired two one-sided test (TOST, equivalence interval: ±1% and ±2 % at 95 % confidence interval).

The feasibility of the sCT-based DRRs for setup verification was analyzed by comparing sCT-DRR-based couch shifts/rotations to the clinically applied ones based on the CT. For the retrospective analysis, first, the sCT image set and its corresponding plan were exported to the ExacTrac system. A DRR based on the sCT was generated (referred to as DRR_{sCT}). The recorded X-ray images from the treatment of each patient were already aligned with the DRRs generated from CT (referred to as DRR_{CT}) during the clinical treatment, and the clinical couch shift for each fraction was recorded in the system. Both the clinical DRR_{CT}-X-ray and the retrospective DRR_{sCT}-X-ray registration were done fully automatic based on the bony structure, and the same settings were used for both registrations. The repeatability of the clinical DRR_{CT} – X-ray differences was evaluated using the calculated residual couch shift from a second X-ray image after the couch correction had been applied, where the overall repeatability was calculated as the mean of these residual couch shifts over all fractions and all patients. Statistical analysis was performed using TOST (95 % confidence interval, equivalence interval: ±1 mm for couch shift, and ± 1° for couch rotation). All statistical analysis was done using Python (Python Software Foundation, Wilmington, United States).

3. Results

3.1. HU values and dosimetric analysis

MAE for HU values between sCT and CT were 135.8 ± 12.9 HU, where the largest differences were found at the bone/soft tissue and soft tissue/air interface.

Table 2, Fig. 2, and Fig. 3 show the results of the dosimetric analysis. Mean ΔD_{50} of PTV and GTV ranged between −0.2 % and 0.2 % (−0.1 to 0.1 Gy), while for OARs mean ΔD_{50} and $\Delta D_{0.01ccm}$ ranged between –0.6 % and 1.6 % (–0.1 to 0.1 Gy) and –1.4 % to 1.0 % (−0.1 to 0.1 Gy), respectively. Both, recalculation of sCT plan on CT and vice versa were equivalent regarding D_{50} and $D_{0.01ccm}$ for target volumes and OARs at ±2 % equivalence interval ($p < 0.001$). When using ±1 % equivalence interval, dose distributions were not all equivalent ($0.05 < p < 0.18$ for GTV and OAR (e.g. chiasma and cochlea) comparisons). The mean difference in CI was found to be in the order of 0.3 %.

Supplementary Figure S1 shows example patients (P02 and P14) who received a bone flap as part of the surgical treatment. Even for these patients, the dosimetric parameters did not differ significantly. For 8 of 9 patients, the bone flap structures were reinserted back to the skull, and were located inside of the PTV. The PTV size of these patients ranged from 19 cc to 1915.4 cc (whole brain RT). For one patient (P02), the bone flap was not reinserted, while the center of the PTV was approximately 3 cm away from the center of the missing skull structure.

3.2. 2D/2D kV-Xray patient setup verification

In total, 25 out of 26 patients (255 fractions) were evaluated. One patient was excluded (P04) due to a technical error during plan export. The contrast of the sCT was sufficient for the automatic rigid registration with the recorded X-ray images (Fig. 4(a)). In the DRR_{CT}, CT markers could be seen and were used for the patient pre-positioning in the clinical routine. No markers were used for sCT for the retrospective evaluation of DRR_{sCT}.

Fig. 4(b) shows the couch shift and rotation differences in the lat./long./vert. direction. The median differences were 0.3 mm/0.2 mm/0.3 mm (95th percentile = 1.2 mm/1.1 mm/2.0 mm, *p*-value: <0.001/<0.001/<0.001) for couch shift and −1.5°/0.1°/0.1° (95th

Table 2
The mean deviation of D_{50}, $D_{0.01}$ [%/cGy] and conformity index (CI) [%] of all 26 patients for planning target volume (PTV), gross tumor volume (GTV), and organ-at-risks.

Mean	PTV	GTV	Brainstem	Chiasma	Opt. nerve (L)	Opt. nerve (R)	Ac. Nerve (L)	Ac. Nerve (R)	Cochlea (L)	Cochlea (R)
ΔD_{50} ($TP_{CT\rightarrow sCT}$) [%/Gy]	0.2/0.1	0.2/0.1	0.6/0.0	1.0/0.1	0.0/0.0	0.1/0.0	0.3/0.0	0.1/0.0	1.6/0.0	0.3/0.1
ΔD_{50} ($TP_{SCT\rightarrow CT}$) [%/Gy]	−0.2/-0.1	−0.2/-0.1	−0.4/0.1	−0.6/0.1	0.0/0.0	0.3/0.0	−0.1/0.0	−0.3/0.0	−0.2/0.0	−0.6/0.0
$\Delta D_{0.01}$ ($TP_{CT\rightarrow sCT}$) [%/Gy]	–	–	0.3/0.1	−0.6/0.1	−0.9/0.1	−0.3/0.1	−0.6/0.0	0.6/0.0	0.1/-0.1	−0.3/0.0
$\Delta D_{0.01}$ ($TP_{SCT\rightarrow CT}$) [%/Gy]	–	–	−1.4/-0.1	−0.9/-0.1	1.0/-0.1	0.2/-0.1	−0.2/0.0	−0.3/0.0	0.2/0.0	−0.4/0.0
Δ CI ($TP_{CT\rightarrow sCT}$)	0.3 %	–	–	–	–	–	–	–	–	–
Δ CI ($TP_{SCT\rightarrow sT}$)	0.3 %	–	–	–	–	–	–	–	–	–

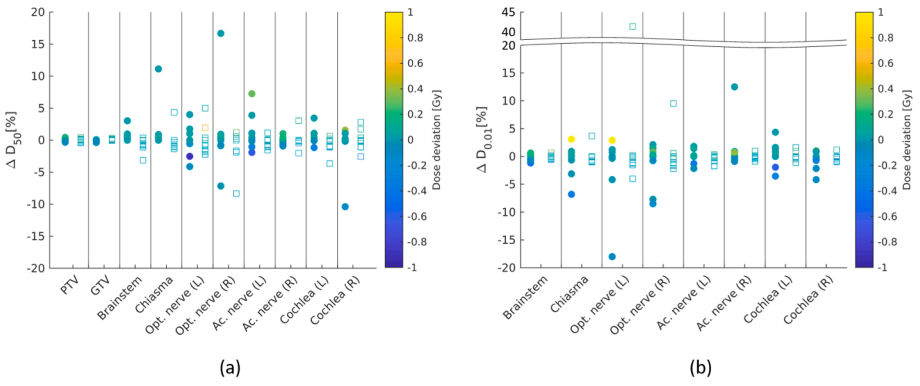

Fig. 2. Dosimetric evaluation of sCT-based plan compared to CT-based plan. (a) Percentage deviation of D_{50} (ΔD_{50}[%]) of target volumes and organ-at-risks (OAR); and (b) percentage deviation of $D_{0.01ccm}$ ($\Delta D_{0.01}$[%]) of OARs. The color bar represents the dose deviation. Values for $TP_{CT\rightarrow sCT}$ are indicated with circular (filled) markers, whereas $TP_{sCT\rightarrow CT}$ are indicated with rectangular (unfilled) markers.

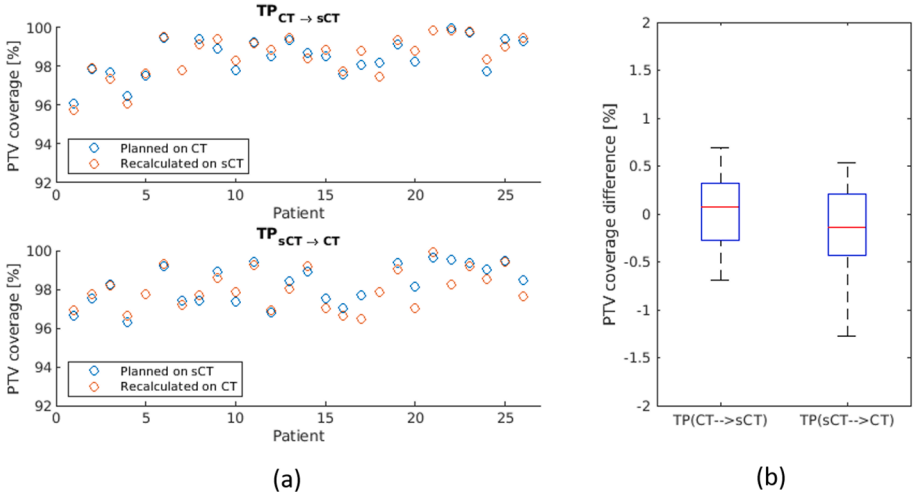

Fig. 3. Evaluation of PTV coverage of sCT-based plan compared to CT-based plan. (a) The PTV coverage (conformity index (CI)) of $TP_{CT\rightarrow sCT}$ and (b) of $TP_{sCT\rightarrow CT}$; (b) the PTV coverage differences between planned and recalculated dose using the two evaluation methods.

percentile = 4.6°/1.8°/1.4°, *p*-value: 0.82/<0.001/<0.001) for the rotations in lat./long./vert. direction. Comparing the subgroups P01-P20 and *P*21-P25 showed the improvement: median rotations in lat./long./vert. of −1.9°/0.3°/0.3° (95th percentile = 4.7°/2.0°/1.6°, *p*-values: 0.42/<0.001/<0.05) improved to −0.4°/−0.1°/−0.4° (95th percentile = 0.2°/1.7°/1.3°, *p*-values: <0.001/<0.001/<0.05) (see Supplementary Figure S2 for details). For the repeatability of the DRR_{CT}-X-ray differences, the calculated mean residual shift/rotation for all patients was -0.1 ± 0.2 mm for couch shift, and $-0.1 \pm 0.3°$ for couch rotation.

To also evaluate the couch rotation difference without the influence of the systematical error in the rotational direction, the rotation difference between sCT and CT image of each patient were first subtracted from the calculated DRR_{sCT} - X-ray rotation for each fraction. The rotation difference was obtained after a rigid registration between sCT and CT image. The median couch rotation differences after the removal of the systematic error in lat./long./vert. were $0.3 \pm 0.7°/-0.1 \pm 0.5°/-0.2 \pm 0.6°$. Overall, the absolute median of shift and rotation differences after the subtraction of the systematic error caused by the setup rotation difference were <1 mm/1°.

4. Discussion

To evaluate the feasibility of the AI-based sCT, following evaluations were conducted: HU-values differences, dose differences, as well as

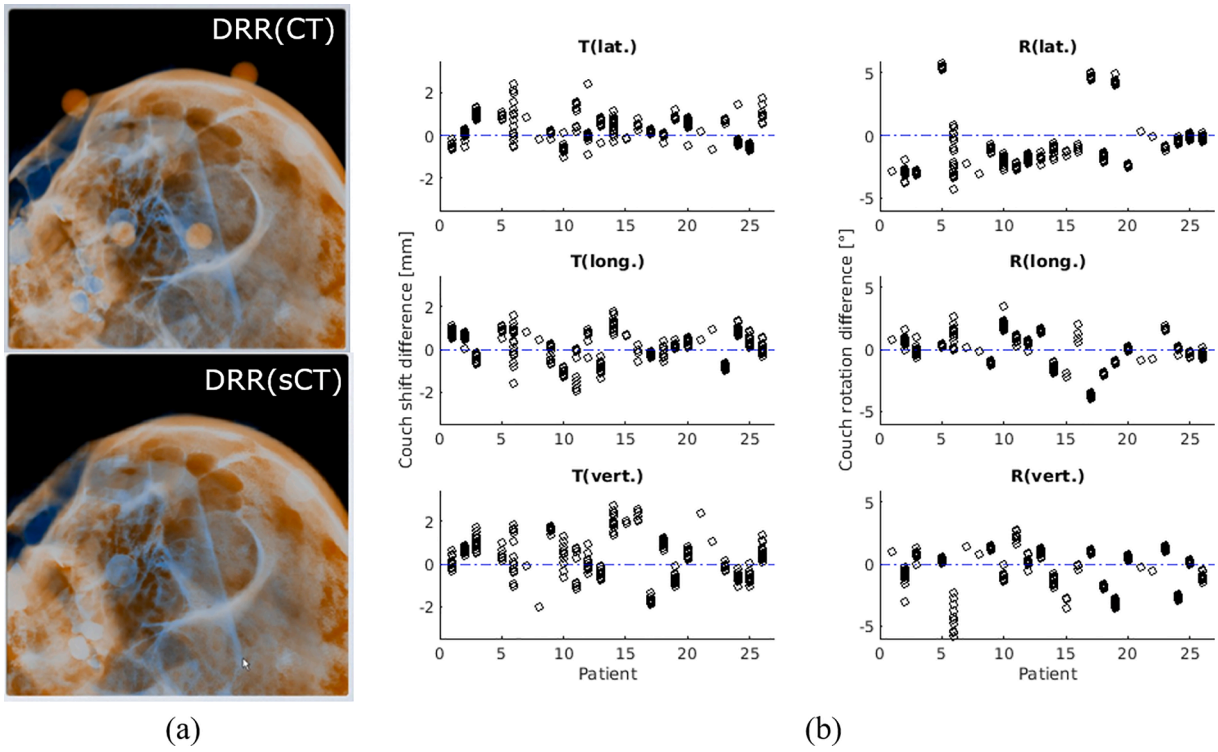

Fig. 4. Comparison of sCT-based DRR and CT-based DRR on the 2D/2D kV-X-ray-based patient setup verification system. (a) DRR-X-ray registration at ExacTrac system using CT (top) and sCT (bottom). (b) (Left) couch shift difference (T: translation) and (right) couch rotation difference (R: rotation) for each patient in lateral, longitudinal, and vertical direction. Blue dashed line represents the 0 value (no deviation). (For interpretation of the references to color in this figure legend, the reader is referred to the web version of this article.)

couch shift/rotation differences. *MAE* for HU values between sCT and CT were 135.8 ± 12.9 HU. Both, recalculation of sCT plan on CT and vice versa were equivalent regarding D_{50} and $D_{0.01ccm}$ for target volumes and OARs at ±2 % equivalence interval ($p < 0.001$). The median differences were <1 mm for couch shift and −1.5°/0.1°/0.1 for the rotations in lat./long./vert. direction. The improvement of RT setup reduced the differences of median rotations in lat./long./vert. of −1.9°/0.3°/0.3° to −0.4°/−0.1°/−0.4°.

MAE has been widely used to evaluate the HU-values differences between CT and sCT, where *MAE* ranging from 120 to 150 HU were reported for the brain [32–35]. Likewise, the *MAE* evaluated for the AI-based sCT in this study was also found to be in this range. The largest deviations were found at the bone/soft tissue as well as soft tissue/air interfaces, which were mostly caused by sCT-CT registration inaccuracy. In this study, the voxels outside the body were excluded, which increased the evaluation accuracy. No dosimetrically significant difference was found between the CT-based plan and sCT-based plan. Dosimetric significance was defined as ±2 %, considering the absolute dosimetry uncertainty was stated to be 2 % for MV photon [36,37]. This dosimetric significance had also been used as dose agreement criteria in other sCT dose evaluation studies [15,38]. For the smallest fractionation in our patient cohort (1x1.8 Gy), this equals 0.36 Gy. All differences in the evaluated dose evaluation metrics fell below the defined dosimetric significance level of ±2 %. Thwaites et al. [39] suggested a dosimetric accuracy of ±1 % of any component of the radiotherapy workflow. The use of MR-only workflow reduced the geometric uncertainty caused by registration. Nonetheless, as observed when using ±1 % as equivalence interval, the dose inaccuracy increased. The D_{50} and $D_{0.01ccm}$ in GTV and several OARs were outside the ±1 % equivalence interval. Several factors can introduce errors in the dose comparison, e.g. dose grid size, plan complexity, the size of PTV, etc, but their specific impacts are out of the scope of this study. All things considered, especially for stereotactic radiosurgery (SRS) where the geometric accuracy is crucial, a dosimetric uncertainty of 2 % is acceptable in an MR-only workflow since a higher geometric accuracy can be achieved.

The two-way validation was necessary for comparing the calculated dose of CT plans and sCT plans. Additionally, evaluating the comparison in the other direction ($TP_{sCT \rightarrow CT}$) could prevent evaluation bias, which had also been done in several works [15,40]. In our evaluation, it was shown that $\mathbf{TP_{CT \rightarrow sCT}}$ and $TP_{sCT \rightarrow CT}$ delivered different results, however, the difference was dosimetrically insignificant. For the 9 patients who had a preceding surgery, the altered bone structure was not reconstructed accurately in the sCT, in both cases when either the bone flap was reinserted or entirely removed (Supplementary Figure S1). This addresses a possible limitation of the AI-based sCT to accurately recognize atypical anatomy, which had also been addressed by Lerner et al. [19], where atypical anatomy in the skull due to surgery using another deep-learning based sCT generation software was investigated using the $TP_{CT \rightarrow sCT}$ method. According to their findings, however, no significant dosimetric impact was found for those patients. In our study, also no significant dosimetric impact was found in this group, even when the altered bone structures were included in the PTV. The PTVs were in these cases large, and the bone flap was mostly reinserted, which explained the small dose difference between sCT and CT plans. In cases with reinserted bone flaps, although sCT reconstruction was not accurate, it only falsely reconstructed the slight gaps around the bone flap while still correctly recognizing the reinserted bone. Even when the PTV was located far enough from the altered structure, as in the case with one patient, this also did not lead to a significant dose difference. Regardless, this effect on the atypical anatomy should be investigated further, i.e. by conducting a study including post-surgery patients with small PTV and assessing whether the dose comparison is influenced by PTV size and distance to the altered bone structure.

There are no unified evaluation metrics and methods for the evaluation of sCT [23,32]. In this study the evaluation metrics were based on the metrics used for institutional clinical guidelines in University Hospital Erlangen (PTV coverage, $D_{50,}$ and $D_{0.01ccm}$). Other studies had used other metrics such as mean dose [15], gamma analysis [20,41], or PTV

coverage [41]. In this study, we found that differences between CT- and sCT-based plans were dosimetrically acceptable. The mean difference in CI was found to be in the order of 0.3 %. In comparison, other deep learning-based sCTs reported dosimetric differences between sCT and CT of <1 % in the PTV [22,42]. Demol et al. [38] evaluated a hybrid atlas-based method for sCT generation for intracranial stereotactic radiosurgery and found a ΔD_{50} of −0.4 % for PTV. We showed that with the AI-based sCT, the ΔD_{50} was improved. For future studies, the sCT-based treatment could be investigated further for non-ideal patients, e.g. patients with metal artifacts, etc.

For the clinical implementation of sCT for MRI-only RT planning, it was necessary to acquire MRI in an optimal RT setup. The median couch shift/rotation difference corresponded directly to the rotational difference of sCT and CT image, which was obtained after the rigid registration of both images. DRR_{sCT} delivered similar results to DRR_{CT} regarding 2D/2D kV-image-based daily positioning after the removal of the positioning errors due to the variation of the RT setup during the MRI scan. While this slight systematic variation did not have impact on the MRI-CT registration accuracy [3], it led to inaccuracies when using kV-image-based positioning as shown in our evaluation data, where we found that the DRR_{sCT} was inequivalent to DRR_{CT} in lateral rotational direction. We found that the two 18 channels flexible coils underneath the RT table-top sometimes led to variation in the rotational lateral direction since they can elevate the cranial part of the RT table-top. To mitigate this problem, additional fixations were added to the sides of the mask holder. For the last 5 patients the variation of rotational angle in yaw and roll direction was more restricted and hence the rotational difference between sCT and CT was minimized. As a result, the accuracy of daily positioning using DRR_{sCT} was improved, and we found that the DRR_{SCT} was equivalent to DRR_{CT} in all translational and rotational directions. The repeatability of the clinical daily positioning using DRR_{CT} was found to be −0.1 mm (shift) and −0.1° (rotation), which is within the clinically acceptable threshold. In comparison, the median differences of calculated shift between DRR_{sCT}- and DRR_{CT}-based daily positioning were slightly larger than the clinical couch shift repeatability, nonetheless still < 1 mm. Likewise, the median differences of calculated couch rotation were larger than the clinical couch rotation repeatability, but still < 1° for the subgroup P21-P25. This implied that when the geometric accuracy of the RT setup was assured, the differences between DRR_{sCT}- and DRR_{CT}-based daily positioning were acceptable for clinical daily positioning. Thus, a meticulous patient setup between MRI and RT should consistently be assured and resulted in our case to further improvement of the RT setup during MRI acquisition. Nevertheless, these found differences might have to be further evaluated and considered for the determination of PTV margin for an sCT-based MRI-only workflow, which is outside the scope of this study. Generally, an intrafractional variability in RT mask must also be considered, which can account for <3° in the rotational direction [43]. Other uncertainties in comparison of CT- and sCT-based RT plans can originate from the inaccuracies of rigid registration between the sCT and CT [1], but they were minimized by using an optimal automatic registration method and the use of a RT setup [3].

Lastly, the limitations of the sCTs regarding its accuracy can stem from the MR-related distortions, e.g. gradient non-linearity and susceptibility-induced distortions [44–46]. The distortion is particularly large in regions away from the isocenter, and hence makes sCT less geometrically accurate compared to CT and impacts the sCT-based dose calculation accuracy. While all MR scanners are equipped with gradient non-linearity distortion correction algorithms, residual distortion can still be present. Nonetheless, this effect is less critical in regions with a small field-of-view, such as the head [47]. Susceptibility-induced distortions have also been investigated for a 1.5 T scanner in the brain where they contribute a median distortion between 0.13 mm and 0.18 mm for different OARs, which is mostly negligible [48].

The advantages of the AI-based sCT over other sCT generation methods lie in the shorter acquisition time (~3m, in comparison to the previous brain sCT solution using the voxel-based technique by the same vendor: ~14 m), which in turn improves patient convenience. When using the voxel-probability assignment-based sCT generation technique, acquiring various sequences including a UTE sequence for bone visibility was necessary, which prolonged the scan and in some cases, was hard to implement clinically.

Even though in the preliminary evaluation the sCT-based plans performed similarly to the CT-based plans, several adjustments must be made before using sCT clinically. Some auxiliary structures which need to be considered for RT planning, e.g. the RT mask, mask holder, and RT table, were not visible in the sCT and could also not be included in MRI due to metal or other MRI-incompatible components. One limitation of this study was that it did not consider these auxiliary structures in the dose calculation and comparison. Nonetheless, these structures could be added to the sCT images in the treatment planning system before the dose calculation, for example by attaching MR-visible markers to the mask holder to determine its position in the MRI images relative to the patient. A dosimetric study with defined auxiliary structures which are considered in the dose calculation and comparison can provide additional value. Similarly, IR-visible markers on the mask used for prepositioning the patient in an ExacTrac workflow need to be substituted. Either ExacTrac is used by using the horseshoe-shaped positioning device attached to the treatment couch or MRI-visible IR-markers e.g. made of silicone can be used to define the IR-markers' position in the MRI, which can then be transferred onto the sCT.

All things considered, a clinical study using this commercial AI-based sCT for brain RT patients should be conducted in the near future. First, the inclusion criteria should be clearly defined, i.e. whether to include patients with a metal implant, positioning difficulties, resection sites, etc. Second, the quality of the RT protocol and setup at the MRI and the reliability of auxiliary structure definition in TPS should be assured, or at least the inaccuracy tolerances defined. When it can be shown that the sCT- and CT-based plans are equivalent for dose calculation and patient setup verification, this will build confidence amongst clinicians to implement the AI-based sCT for an MRI-only workflow.

In this study, we showed that the commercial deep-learning-based sCT algorithm is comparable to the planning CT regarding dose calculation and daily stereoscopic X-ray positioning when using an optimal RT setup during MRI acquisition, while the HU-differences are within the acceptable range. Hence, this deep-learning-based sCT generation technique offers a promising solution for an MR-only workflow for brain RT.

Declaration of Competing Interest

The authors declare that they have no known competing financial interests or personal relationships that could have appeared to influence the work reported in this paper.

Acknowledgments

The presented work was performed in partial fulfilment of the requirements for obtaining the degree of *Dr. rer. biol. hum.* at Friedrich-Alexander-Universität (FAU).

Appendix A. Supplementary data

Supplementary data to this article can be found online at https://doi.org/10.1016/j.phro.2022.10.002.

References

[1] Putz F, Mengling V, Perrin R, Masitho S, Weissmann T, Rosch J, et al. Magnetic resonance imaging for brain stereotactic radiotherapy : A review of requirements and pitfalls. Strahlenther Onkol 2020;196:444–56. https://doi.org/10.1007/s00066-020-01604-0.

[2] Ulin K, Urie MM, Cherlow JM. Results of a multi-institutional benchmark test for cranial CT/MR image registration. Int J Radiat Oncol Biol Phys 2010;77:1584–9. https://doi.org/10.1016/j.ijrobp.2009.10.017.

[3] Masitho S, Putz F, Mengling V, Reissig L, Voigt R, Bauerle T, et al. Accuracy of MRI-CT registration in brain stereotactic radiotherapy: Impact of MRI acquisition setup and registration method. Z Med Phys 2022. https://doi.org/10.1016/j.zemedi.2022.04.004.

[4] Hanvey S, Sadozye AH, McJury M, Glegg M, Foster J. The influence of MRI scan position on image registration accuracy, target delineation and calculated dose in prostatic radiotherapy. Br J Radiol 2012;85:e1256–62. https://doi.org/10.1259/bjr/26802977.

[5] Hanvey S, McJury M, Tho LM, Glegg M, Thomson M, Grose D, et al. The influence of MRI scan position on patients with oropharyngeal cancer undergoing radical radiotherapy. Radiat Oncol 2013;8:129. https://doi.org/10.1186/1748-717X-8-129.

[6] Paulson ES, Crijns SP, Keller BM, Wang J, Schmidt MA, Coutts G, et al. Consensus opinion on MRI simulation for external beam radiation treatment planning. Radiother Oncol 2016;121:187–92. https://doi.org/10.1016/j.radonc.2016.09.018.

[7] Schmidt MA, Payne GS. Radiotherapy planning using MRI. Phys Med Biol 2015;60:R323–61. https://doi.org/10.1088/0031-9155/60/22/R323.

[8] Kocher M, Wittig A, Piroth MD, Treuer H, Seegenschmiedt H, Ruge M, et al. Stereotactic radiosurgery for treatment of brain metastases. A report of the DEGRO Working Group on Stereotactic Radiotherapy. Strahlenther Onkol 2014;190:521–32. https://doi.org/10.1007/s00066-014-0648-7.

[9] Guckenberger M, Baus WW, Blanck O, Combs SE, Debus J, Engenhart-Cabillic R, et al. Definition and quality requirements for stereotactic radiotherapy: consensus statement from the DEGRO/DGMP Working Group Stereotactic Radiotherapy and Radiosurgery. Strahlenther Onkol 2020;196:417–20. https://doi.org/10.1007/s00066-020-01603-1.

[10] Karlsson M, Karlsson MG, Nyholm T, Amies C, Zackrisson B. Dedicated magnetic resonance imaging in the radiotherapy clinic. Int J Radiat Oncol Biol Phys 2009;74:644–51. https://doi.org/10.1016/j.ijrobp.2009.01.065.

[11] Kristensen BH, Laursen FJ, Logager V, Geertsen PF, Krarup-Hansen A. Dosimetric and geometric evaluation of an open low-field magnetic resonance simulator for radiotherapy treatment planning of brain tumours. Radiother Oncol 2008;87:100–9. https://doi.org/10.1016/j.radonc.2008.01.014.

[12] Wang C, Chao M, Lee L, Xing L. MRI-based treatment planning with electron density information mapped from CT images: a preliminary study. Technol Cancer Res Treat 2008;7:341–8. https://doi.org/10.1177/153303460800700501.

[13] Stanescu T, Jans HS, Pervez N, Stavrev P, Fallone BG. A study on the magnetic resonance imaging (MRI)-based radiation treatment planning of intracranial lesions. Phys Med Biol 2008;53:3579–93. https://doi.org/10.1088/0031-9155/53/13/013.

[14] Hsu SH, Cao Y, Huang K, Feng M, Balter JM. Investigation of a method for generating synthetic CT models from MRI scans of the head and neck for radiation therapy. Phys Med Biol 2013;58:8419–35. https://doi.org/10.1088/0031-9155/58/23/8419.

[15] Paradis E, Cao Y, Lawrence TS, Tsien C, Feng M, Vineberg K, et al. Assessing the dosimetric accuracy of magnetic resonance-generated synthetic CT images for focal brain VMAT radiation therapy. Int J Radiat Oncol Biol Phys 2015;93:1154–61. https://doi.org/10.1016/j.ijrobp.2015.08.049.

[16] Korhonen J, Kapanen M, Keyrilainen J, Seppala T, Tenhunen M. A dual model HU conversion from MRI intensity values within and outside of bone segment for MRI-based radiotherapy treatment planning of prostate cancer. Med Phys 2014;41:011704. https://doi.org/10.1118/1.4842575.

[17] Johansson A, Karlsson M, Yu J, Asklund T, Nyholm T. Voxel-wise uncertainty in CT substitute derived from MRI. Med Phys 2012;39:3283–90. https://doi.org/10.1118/1.4711807.

[18] Han X. MR-based synthetic CT generation using a deep convolutional neural network method. Med Phys 2017;44:1408–19. https://doi.org/10.1002/mp.12155.

[19] Lerner M, Medin J, Jamtheim Gustafsson C, Alkner S, Siversson C, Olsson LE. Clinical validation of a commercially available deep learning software for synthetic CT generation for brain. Radiat Oncol 2021;16:66. https://doi.org/10.1186/s13014-021-01794-6.

[20] Tang B, Wu F, Fu Y, Wang X, Wang P, Orlandini LC, et al. Dosimetric evaluation of synthetic CT image generated using a neural network for MR-only brain radiotherapy. J Appl Clin Med Phys 2021;22:55–62. https://doi.org/10.1002/acm2.13176.

[21] Wang T, Manohar N, Lei Y, Dhabaan A, Shu HK, Liu T, et al. MRI-based treatment planning for brain stereotactic radiosurgery: Dosimetric validation of a learning-based pseudo-CT generation method. Med Dosim 2019;44:199–204. https://doi.org/10.1016/j.meddos.2018.06.008.

[22] Dinkla AM, Wolterink JM, Maspero M, Savenije MHF, Verhoeff JJC, Seravalli E, et al. MR-only brain radiation therapy: dosimetric evaluation of synthetic CTs generated by a dilated convolutional neural network. Int J Radiat Oncol Biol Phys 2018;102:801–12. https://doi.org/10.1016/j.ijrobp.2018.05.058.

[23] Johnstone E, Wyatt JJ, Henry AM, Short SC, Sebag-Montefiore D, Murray L, et al. Systematic review of synthetic computed tomography generation methodologies for use in magnetic resonance imaging-only radiation therapy. Int J Radiat Oncol Biol Phys 2018;100:199–217. https://doi.org/10.1016/j.ijrobp.2017.08.043.

[24] Edmund JM, Andreasen D, Mahmood F, Van Leemput K. Cone beam computed tomography guided treatment delivery and planning verification for magnetic resonance imaging only radiotherapy of the brain. Acta Oncol 2015;54:1496–500. https://doi.org/10.3109/0284186X.2015.1062546.

[25] Buhl SK, Duun-Christensen AK, Kristensen BH, Behrens CF. Clinical evaluation of 3D/3D MRI-CBCT automatching on brain tumors for online patient setup verification - A step towards MRI-based treatment planning. Acta Oncol 2010;49:1085–91. https://doi.org/10.3109/0284186X.2010.498442.

[26] Price RG, Kim JP, Zheng W, Chetty IJ, Glide-Hurst C. Image guided radiation therapy using synthetic computed tomography images in brain cancer. Int J Radiat Oncol Biol Phys 2016;95:1281–9. https://doi.org/10.1016/j.ijrobp.2016.03.002.

[27] Yang Y, Cao M, Kaprealian T, Sheng K, Gao Y, Han F, et al. Accuracy of UTE-MRI-based patient setup for brain cancer radiation therapy. Med Phys 2016;43:262. https://doi.org/10.1118/1.4938266.

[28] Hoesl M, Corral, N. E., Mistry, N. MR-based Synthetic CT. An AI-based algorithm for continuous Hounsfield units in the pelvis and brain - with syngo.via RT Image Suite. MReadings: MR in RT, 8th Edition, ESTRO 2022;30-42. https://www.magnetomworld.siemens-healthineers.com/publications/mreadings.

[29] Mengling V, Bert C, Perrin R, Masitho S, Weissmann T, Mansoorian S, et al. Implementation of a dedicated 1.5T MR scanner for radiotherapy treatment planning featuring a novel high-channel coil setup for brain imaging in treatment position. Strahlenther Onkol 2020;197:246–56. https://doi.org/10.1007/s00066-020-01703-y.

[30] Ma J, Chang Z, Wang Z, Jackie WQ, Kirkpatrick JP, Yin FF. ExacTrac X-ray 6 degree-of-freedom image-guidance for intracranial non-invasive stereotactic radiotherapy: comparison with kilo-voltage cone-beam CT. Radiother Oncol 2009;93:602–8. https://doi.org/10.1016/j.radonc.2009.09.009.

[31] Timmerman R. A story of hypofractionation and the table on the wall. Int J Radiat Oncol Biol Phys 2022;112:4–21. https://doi.org/10.1016/j.ijrobp.2021.09.027.

[32] Edmund JM, Nyholm T. A review of substitute CT generation for MRI-only radiation therapy. Radiat Oncol 2017;12:28. https://doi.org/10.1186/s13014-016-0747-y.

[33] Johansson A, Karlsson M, Nyholm T. CT substitute derived from MRI sequences with ultrashort echo time. Med Phys 2011;38:2708–14. https://doi.org/10.1118/1.3578928.

[34] Zheng W, Kim JP, Kadbi M, Movsas B, Chetty IJ, Glide-Hurst CK. Magnetic resonance-based automatic air segmentation for generation of synthetic computed tomography scans in the head region. Int J Radiat Oncol Biol Phys 2015;93:497–506. https://doi.org/10.1016/j.ijrobp.2015.07.001.

[35] Gudur MS, Hara W, Le QT, Wang L, Xing L, Li R. A unifying probabilistic Bayesian approach to derive electron density from MRI for radiation therapy treatment planning. Phys Med Biol 2014;59:6595–606. https://doi.org/10.1088/0031-9155/59/21/6595.

[36] Ahnesjo A, Aspradakis MM. Dose calculations for external photon beams in radiotherapy. Phys Med Biol 1999;44:R99–. https://doi.org/10.1088/0031-9155/44/11/201.

[37] Korsholm ME, Waring LW, Edmund JM. A criterion for the reliable use of MRI-only radiotherapy. Radiat Oncol 2014;9:16. https://doi.org/10.1186/1748-717X-9-16.

[38] Demol B, Boydev C, Korhonen J, Reynaert N. Dosimetric characterization of MRI-only treatment planning for brain tumors in atlas-based pseudo-CT images generated from standard T1-weighted MR images. Med Phys 2016;43:6557. https://doi.org/10.1118/1.4967480.

[39] Thwaites D. Accuracy required and achievable in radiotherapy dosimetry: have modern technology and techniques changed our views? J Phys Conf Ser 2013;444:012006. https://doi.org/10.1088/1742-6596/444/1/012006.

[40] Jonsson JH, Johansson A, Soderstrom K, Asklund T, Nyholm T. Treatment planning of intracranial targets on MRI derived substitute CT data. Radiother Oncol 2013;108:118–22. https://doi.org/10.1016/j.radonc.2013.04.028.

[41] Jonsson JH, Akhtari MM, Karlsson MG, Johansson A, Asklund T, Nyholm T. Accuracy of inverse treatment planning on substitute CT images derived from MR data for brain lesions. Radiat Oncol 2015;10:13. https://doi.org/10.1186/s13014-014-0308-1.

[42] Liu F, Yadav P, Baschnagel AM, McMillan AB. MR-based treatment planning in radiation therapy using a deep learning approach. J Appl Clin Med Phys 2019;20:105–14. https://doi.org/10.1002/acm2.12554.

[43] Tryggestad E, Christian M, Ford E, Kut C, Le Y, Sanguineti G, et al. Inter- and intrafraction patient positioning uncertainties for intracranial radiotherapy: a study of four frameless, thermoplastic mask-based immobilization strategies using daily cone-beam CT. Int J Radiat Oncol Biol Phys 2011;80:281–90. https://doi.org/10.1016/j.ijrobp.2010.06.022.

[44] Nyholm T, Nyberg M, Karlsson MG, Karlsson M. Systematisation of spatial uncertainties for comparison between a MR and a CT-based radiotherapy workflow for prostate treatments. Radiat Oncol 2009;4:54. https://doi.org/10.1186/1748-717X-4-54.

[45] Baldwin LN, Wachowicz K, Fallone BG. A two-step scheme for distortion rectification of magnetic resonance images. Med Phys 2009;36:3917–26. https://doi.org/10.1118/1.3180107.

[46] Wang H, Balter J, Cao Y. Patient-induced susceptibility effect on geometric distortion of clinical brain MRI for radiation treatment planning on a 3T scanner. Phys Med Biol 2013;58:465–77. https://doi.org/10.1088/0031-9155/58/3/465.

[47] Adjeiwaah M, Bylund M, Lundman JA, Soderstrom K, Zackrisson B, Jonsson JH, et al. Dosimetric impact of MRI distortions: a study on head and neck cancers. Int J Radiat Oncol Biol Phys 2019;103:994–1003. https://doi.org/10.1016/j.ijrobp.2018.11.037.

[48] Mengling V, Putz F, Laun FB, Perrin R, Eisenhut F, Dorfler A, et al. Evaluation of the influence of susceptibility-induced magnetic field distortions on the precision of contouring intracranial organs at risk for stereotactic radiosurgery. Phys Imaging Radiat Oncol 2020;15:91–7. https://doi.org/10.1016/j.phro.2020.08.001.